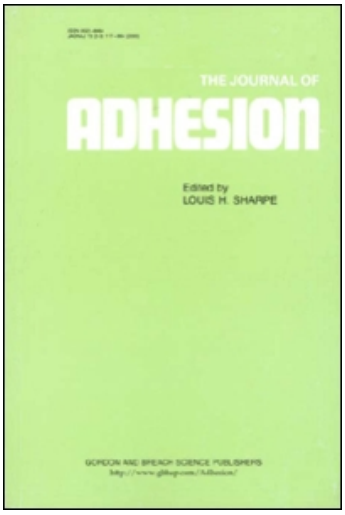

The Journal of Adhesion
Publication details, including instructions for authors and subscription information:
http://www.informaworld.com/smpp/title~content=t713453635

3-D Nonlinear Stress Analysis on Adhesively Bonded Single Lap Composite Joints with Different Ply Stacking Sequences

Murat Demir Aydın[a]
[a] Erzurum MYO, Atatürk Üniversity, Erzurum, Turkey

To cite this Article Aydın, Murat Demir(2008) '3-D Nonlinear Stress Analysis on Adhesively Bonded Single Lap Composite Joints with Different Ply Stacking Sequences', The Journal of Adhesion, 84: 1, 15 — 36
To link to this Article: DOI: 10.1080/00218460801888359
URL: http://dx.doi.org/10.1080/00218460801888359

The Journal of Adhesion, 84:15–36, 2008

ISSN: 0021-8464 print/1545-5823 online
DOI: 10.1080/00218460801888359

Taylor & Francis
Taylor & Francis Group

3-D Nonlinear Stress Analysis on Adhesively Bonded Single Lap Composite Joints with Different Ply Stacking Sequences

Murat Demir Aydın
Erzurum MYO, Atatürk Üniversity, Erzurum, Turkey

A 3-D nonlinear finite element code was established to assess the effects of the fiber orientation angle of the laminates on the stress distributions and the failure prediction in single lap joints (SLJs) subjected to uniaxial tensile loading. Eight different configurations were considered and the unidirectional prepregs were laid up in quasi-isotropic ($[90/\pm45/0]_{2s}$ and $[90/\pm30/90]_{2s}$), cross-ply ($[0/90]_{4s}$ and $[30/60]_{4s}$), angle-ply ($[45/-45]_{4s}$ and $[55/-55]_{4s}$), and unidirectional ($[0]_{16}$ and $[90]_{16}$). The composite adherends (AS4/3501-6) were assumed to behave as linearly elastic materials while the adhesive layer (FM 73) was assumed to be nonlinear. The nonlinear geometric deformations of the SLJs were also taken into account. The first step in the analysis, a complete 3-D stress analysis, is carried out with a special importance for the evaluation of out-of-plane stresses. Then, the failure index distributions are calculated by using the Tsai-Wu failure criterion for composite adherends and the extended Drucker-Prager failure criterion for the adhesive layer. Consequently, it is seen that the state of stress in the vicinity of the free edge of the joint is fully 3-D which has not been taken into account in any classical theory so far and the normal and shear stress distributions are extremely sensitive to these 3-D effects (anti-clastic, free edge, and bending-twisting coupling effects). Hence, in real applications of adhesively bonded composite joints, the out-of-plane stresses and 3-D effects cannot be neglected and a 3-D finite element method is essential to evaluate explicitly the stress and failure states. Also, for both the adherends and the adhesive layer, the ply stacking sequence has a significant effect on the stress distribution and the failure.

Keywords: Adhesive; Composite lap joint; Nonlinear finite element; Ply stacking sequence; Three-dimensional effects

Received 17 August 2007; in final form 13 December 2007.
Address correspondence to Murat Demir Aydın, Erzurum MYO, Atatürk Üniversity, 25240 Erzurum, Turkey. E-mail: mdemira@atauni.tr

1. INTRODUCTION

In advanced engineering structures such as aircraft, spacecraft, automobile transmission shafts, and robot structures, composite materials have found applications because of their high strength/weight ratios and high damping capacity. These applications usually require the joining of composites either to other composites or to metals. Generally, composite structural components are connected with other components by means of a mechanical joint or an adhesively bonded joint. The mechanical joint is fastened by using bolts or rivets, which requires drilling holes. But drilled holes significantly reduce the load carrying capacity of composites due to the stress concentration in the vicinity of the boundary of the hole. This reduction could cause catastrophic failure [1]. Therefore, adhesively bonded joints are more preferable to a mechanical joint in the joining of composite materials [2]. On the other hand, the analysis of adhesively bonded joints requires a reliable and efficient tool to obtain stresses, strains, and fracture parameters.

The stress analysis on an adhesively bonded joint is typically performed in one of two ways: analytical modeling (closed-form) and numerical solution. In the first approach, a set of differential equations and boundary conditions is formulated. The solutions of these equations are analytical expressions which give values of stresses at any point of the joint. Several analytical models have been developed for analysis of adhesively bonded joints [2–11]. Historically speaking, one would cite the work of Goland and Reissner [4] as one of the earliest investigations performed on the cylindrical bending plate analysis of a single lap joint (SLJ). Since then several workers performed work on this subject; for instance, Hart-Smith [5] developed a layered beam model to solve the SLJ problem. Oplinger [6] also developed a beam method by considering the overlap bending moments and introducing the individual tensile forces in the upper and lower adherends at the overlap section. In order to ensure that the stress-free boundary conditions would be satisfied at the free ends, some researchers employed 2-D elasticity theory in conjunction with the variational method, such as minimum strain method [7,8] and the principle of complementary energy method [9]. A 2-D elasticity based solution was also presented by Tsai *et al*. [10]. In the analyses used in the quoted references, the peel and shear stresses are assumed constant across the adhesive thickness; the shear is maximum at the overlap ends and the adherends are assumed to deform only in tension [12].

In the second approach, solutions of differential equations are obtained by numerical methods. Firstly, a system of algebraic

equations is derived, generally from energy functionals. The solution of these equations gives displacements at determined points from which strains and stresses can be obtained for any point within the model. Numerical methods provide a general tool for analysis of arbitrary geometries and loading conditions. Among the numerical methods, the finite element method (FEM) has been extensively used with success and countless studies on the various adhesively bonded joints via this technique were performed by many authors [12–24].

On the other hand, unlike the isotropic adherend, laminated composite adherends have relatively low transverse strength and shear stiffness compared with the in-plane material properties. Also, laminates suffer from material non-homogeneity, residual stresses, and free edge problems. These factors make the problem of adhesively bonded joints with composite adherends more complex than that with homogeneous isotropic adherends [25,26]. Thus, the 3-D analysis is essential for understanding the joint stress fields, damage initiation, and its propagation in practical applications. But the 3-D stress and failure prediction for bonded joints is a difficult analytical problem, owing to the fact that an adequate solution has to account for the step-wise geometry and material property variations, anisotropy, and laminated construction of the adherends, nonlinear behavior of adhesive, etc. [27,28].

The use of the FEM to study adhesively bonded joints with composite adherends has brought a new level of understanding of these structures. However, there is a very little work in the literature regarding the complete tri-axial stress state, the effects of the stacking sequence of the laminates on the stress distributions, damage prediction, and its propagation [26–31].

In the present study, a 3-D nonlinear finite element code is established to analyze the effects of the stacking sequence of the laminates on the stress distributions and the failure prediction in the SLJs with composite adherends subjected to uniaxial loadings.

2. NUMERICAL MODELING

In order to demonstrate the effect of stacking sequence on the stress distributions in SLJs with composite adherends subjected to uniaxial loadings the SLJs can be separated into its two main constituents: the composite adherends and the adhesive bond-line.

In the analyses dealing with orthotropic materials, the anisotropic criteria of yielding have to be considered. For engineering applications, those criteria should adequately describe the behavior of a material and should have simple forms, allowing one to determine

their parameters by simple strength tests. Therefore, under the 3-D stress states in the overlap region, the failure generally can be evaluated by the Tsai-Wu quadratic failure criterion which takes into account the interaction of all six stress components and this criterion can be expressed as follows [32]:

$$e_{com} = A + B + C \quad \begin{cases} e_{com} < 1; & \text{no failure} \\ e_{com} \geq 1; & \text{failure} \end{cases} \tag{1}$$

$$A = -\frac{\sigma_{11}^2}{S_{11}^t S_{11}^c} - \frac{\sigma_{22}^2}{S_{22}^t S_{22}^c} - \frac{\sigma_{33}^2}{S_{33}^t S_{33}^c} + \left(\frac{\sigma_{12}}{S_{12}}\right)^2 + \left(\frac{\sigma_{23}}{S_{23}}\right)^2 + \left(\frac{\sigma_{13}}{S_{13}}\right)^2,$$

$$B = -\frac{\sigma_{11}\sigma_{22}}{\sqrt{S_{11}^t S_{11}^c S_{22}^t S_{22}^c}} - \frac{\sigma_{22}\sigma_{33}}{\sqrt{S_{22}^t S_{22}^c S_{33}^t S_{33}^c}} - \frac{\sigma_{11}\sigma_{33}}{\sqrt{S_{11}^t S_{11}^c S_{33}^t S_{33}^c}},$$

$$C = \left(\frac{1}{S_{11}^t} + \frac{1}{S_{11}^c}\right) \cdot \sigma_{11} + \left(\frac{1}{S_{22}^t} + \frac{1}{S_{22}^c}\right) \cdot \sigma_{22} + \left(\frac{1}{S_{33}^t} + \frac{1}{S_{33}^c}\right) \cdot \sigma_{33}$$

Here σ_{ij}, S_{ij}, and e_{com} are the stress components referred to the principal material's coordinates, the strength components of the composite material, and the failure index for composite adherends, respectively. Also, superscripts c and t denote compression and tension.

On the other hand, an adhesive exhibits a nonlinear relationship between stress and strain. Hence, for the purpose of finite element analysis, elastic-plastic models have been used to describe the deformation behavior. The onset of nonlinearity in the stress-strain curve is due to plastic deformation and it occurs at the first yield stress. The subsequent increase in stress with strain is related to the effects of strain hardening, and stress calculations involve the use of a yield criterion. Also, the plastic yielding behavior in polymers such as adhesives is well known to be sensitive to the hydrostatic pressure and, thus, a pressure-dependent yield criterion is often used [33–42]. Drucker-Prager [33] and Raghava [34] criteria both account for hydrostatic pressure sensitivity in materials. In the study, the Raghava criterion given as follows, was used:

$$(\sigma_1 - \sigma_2)^2 + (\sigma_2 - \sigma_3)^2 + (\sigma_3 - \sigma_1)^2 + 2 \cdot (\sigma_c - \sigma_t) \cdot (\sigma_1 + \sigma_2 + \sigma_3) = 2 \cdot \sigma_c \cdot \sigma_t \cdot e. \tag{2}$$

Here σ_1, σ_2, and σ_3 are the principal stresses causing yield and σ_c and σ_t are the absolute values of uniaxial compressive and tensile yield stresses of the adhesive material, respectively. This criterion can differently be written

$$\frac{q^2}{\lambda \cdot \sigma_t^2} + \frac{3\sigma_t(\lambda - 1) \cdot \sigma_m}{\lambda \cdot \sigma_t^2} = e \quad \begin{cases} e \geq 1 & \text{failure} \\ e < 1 & \text{no failure} \end{cases} \tag{3}$$

$$q^2 = \frac{1}{2}\left[(\sigma_1 - \sigma_2)^2 + (\sigma_2 - \sigma_3)^2 + (\sigma_3 - \sigma_1)^2\right] = 3J_2 \tag{3a}$$

$$\sigma_m = \frac{J_1}{3}, \tag{3b}$$

where J_1, J_2, and q are the first invariant of the stress tensor, the second invariant of the deviatoric stress tensor and the von-Mises equivalent stress, respectively, and e is the failure index for a film type adhesive. Also, λ is the hydrostatic stress sensitivity parameter and relates yield stresses σ_t, σ_c, and τ_y under uniaxial tension, compression, and shear given by the following equations [36–41]:

$$\lambda = \frac{\sigma_c}{\sigma_t}; \quad \lambda = \frac{\sigma_c^2}{3\tau_y^2}; \quad \lambda = \frac{3\tau_y^2}{\sigma_t^2}. \tag{4}$$

The Raghava criterion exists in the finite element package ANSYS 10.0 (ANSYS, Inc., Canonsburg, PA, USA) [35] as the "extended Drucker-Prager" model and is described by the Eq. (5):

$$q^b + \alpha\sigma_m = \sigma_t^b, \tag{5}$$

where α and σ_m are the material parameter referred to the pressure sensitive parameter and mean or hydrostatic stress, respectively. Also, b is the material parameter characterizing the shape of the yield surface. Assuming the special case of $b = 2$, rearranging and comparing with Eq. (3), the following relationship for α can be derived:

$$\alpha = 3\sigma_t(\lambda - 1). \tag{6}$$

The data needed for this elastic-plastic model are elasticity modulus of adhesive (E_a), the elastic component of Poisson's ratio (ν_e), α, dilation angle (ψ), and the tensile strain hardening function $\sigma_t\varepsilon_t^p$. The dilation angle (ψ) describes the orientation of the plastic flow vector and this is calculated from the plastic component of Poisson's ratio, ν_p, given as follows [36–41]:

$$\tan\psi = \frac{3(1 - 2\nu_p)}{2(1 + \nu_p)}. \tag{7}$$

2.1. Modeling Data for the Adhesive and the Composite Adherends

The film-type adhesive being studied is FM 73 (Cytec, Ostringen, Germany). It is a high-strength, rubber-modified, general purpose

aerospace epoxy designed to provide excellent structural performance from -55°C to 82°C. The manufacturer's suggested cure cycle is 1 h at 120°C at 300 kPa pressure.

The stress-strain behaviors of adhesives under shear, tension, or compression are necessary for the elastic-plastic stress analysis mentioned above *via* nonlinear FEM. For this purpose, bulk specimens from the adhesive used in this study were prepared as follows:

- In order to adjust the thickness of the bulk specimens, a U-shaped spacer frame, as seen in Fig. 1a, was fixed onto the lower plate of a hot press used for curing the adhesive. The height of the frame determines the specimen thickness and a height of 2 to 3 mm is suitable for most tests [43,44]. Therefore, a spacer frame 2 mm in thickness was used.
- A release agent was applied to the upper and lower plates of the hot press, so as to easily separate the cured adhesive from the upper and lower platens of the hot press.
- The layers were stacked, after the film adhesive was cut to ten layers.
- In order to prevent any entrapment of air between the adhesive layers and for curing the stacked film adhesives, the pressure was applied with the upper and lower platens of a hot press, which were at 120°C for FM 73. After curing, bulk specimens were machined to the dimensions shown in Fig. 1b [45].

The stress-strain ($\sigma-\varepsilon$) behavior of the adhesives was determined from bulk dumb-bell specimens tested under ambient conditions at room temperature. Four specimens were tested to failure at a

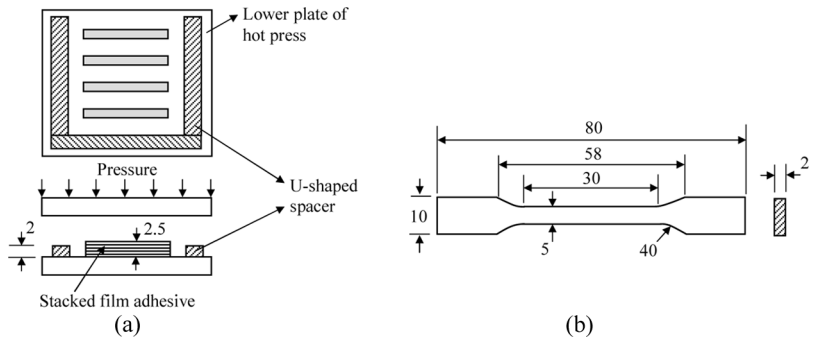

FIGURE 1 Preparation of the bulk specimens: (a) hot press and stacked film adhesive and (b) tensile test specimen [21] (all dimensions in mm).

TABLE 1 Material Parameters for the Exponent Drucker-Prager Model (FM 73)

E_a (MPa)	ν_e	λ	α (MPa) (Eq. 6)	ν_p	$\tan\psi$ (Eq. 7)	$\sigma_y(\bar{\varepsilon}^{pl})$
2160	0.35	1.63	96.39	0.27	0.54331	see Fig. 2

crosshead speed of 1 mm/min [46]. For determination of the elastic properties (E_a and ν_e) given in Table 1, longitudinal and transverse strains were measured using two SG25-50CA clip-on extensometers (Shimadzu Corporation, Tokyo, Japan).

For determining the tensile curve, strains were measured using a Shimadzu DVE-100/200 video extensometer (Shimadzu Corporation, Tokyo, Japan). Later, the tensile hardening function, $\sigma_t(\varepsilon_t^p)$, was obtained from the tensile curve by subtracting the elastic strain component from each value of the total tensile strain. Finally, the resulting curve was developed and is presented in Fig. 2.

The parameter α is calculated from Eq. (6). This requires a knowledge of the parameter λ. Thus, λ can be calculated from yield stresses obtained at the same equivalent plastic strain ($\bar{\varepsilon}^{pl}$) and measured under two different stress states (tension/compression, tension/shear, or compression/shear). If the shear data are available, then the relation between yield stress at tension and yield stress at shear must

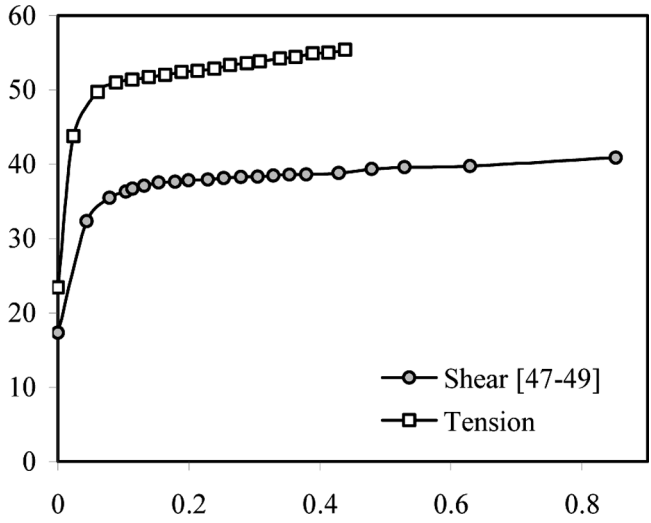

FIGURE 2 True stress-true plastic strain behaviors of adhesive (FM 73) under tension and shear.

be known. For pure shear loading conditions where a shear stress τ_y is applied, the stress invariants are equal to $J_1 = 0$ and $J_2 = \tau_y^2$. Thus, Eq. (3) can be written as [41]:

$$\frac{\sigma_t}{\tau_y} = \sqrt{\frac{3}{\lambda}}. \tag{8}$$

In order to proceed further, the equivalent plastic strain relationships, $\bar{\varepsilon}^{pl}$, are required, *i.e.,* the yield criteria need to be re-written in terms of strain invariants (J_1', J_2'). Hence [41],

$$\bar{\varepsilon}^{pl} = \frac{\lambda - 1}{2\lambda \cdot (1 - 2\nu_p)} \cdot J_1' + \frac{1}{2\lambda} \cdot \sqrt{\frac{(\lambda - 1)^2}{\cdot (1 - 2\nu_p)^2} \cdot (J_1')^2 + \frac{12\lambda}{(1 + \nu_p)^2} \cdot J_2'}. \tag{9}$$

For the uniaxial tensile loading, $\bar{\varepsilon}^{pl}$ is equal to the tensile plastic strain (ε_t) and also for pure shear loading conditions, the strain invariants are equal to $J_1' = 0$ and $J_2' = \gamma_y^2/4$. Thus, the following relationship for $\bar{\varepsilon}^{pl}$ can be derived:

$$\bar{\varepsilon}^{pl} = \frac{\sqrt{3} \cdot \gamma_y}{2\sqrt{\lambda} \cdot (1 + \nu_p)} = \varepsilon_t. \tag{10}$$

Consequently, the following relationship between the tensile secant slope $(S_t = \frac{\sigma_t}{\varepsilon_t})$ and the shear secant slope $(S_s = \frac{\tau_y}{\gamma_y})$ by using Eqs. (8) and (10) is obtained:

$$S_s = \frac{S_t}{2(1 + \nu_p)}. \tag{11}$$

For this study, the shear stress-strain behavior of the film type adhesive (FM 73) obtained from the Thick Adherend Shear Test (TAST) reported earlier in references [47–49] was used and the values of λ were determined from a combination of tension and shear tests as follows:

- Calculate the tensile secant slope $(S_t = \frac{\sigma_t}{\varepsilon_t})$.
- Calculate the shear secant slope by using Eq. (11).
- Determine the values of τ_y and γ_y such that $S_s = \frac{\tau_y}{\gamma_y}$. This ensures the same equivalent plastic strain.
- Calculate the parameters λ and α by using Eqs. (8) and (6), respectively.

Figures 3a and 3b show the change of the parameter λ with the plastic strain and the change of the pressure sensitive parameter (α)

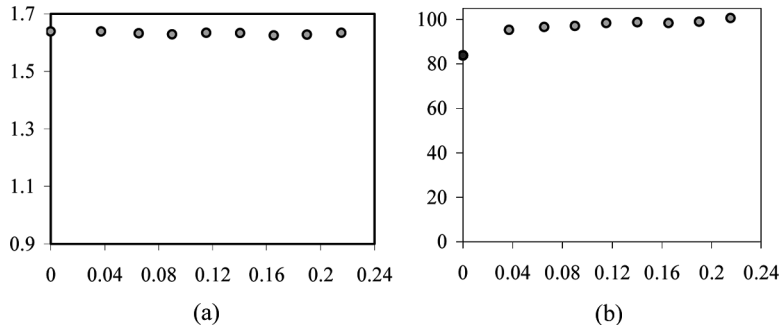

FIGURE 3 (a) Change of the parameter λ with the plastic strain and (b) change of the pressure sensitive parameter (α) with the plastic strain.

with the plastic strain, respectively. It is seen from Fig. 3b that α changes between 83 and 100. In the study, the α value was obtained from the average of values between 83 and 100. Finally, the exponent Drucker-Prager (Raghava) material constants (λ, α, and ψ) for FM 73 are given in Table 1.

Also, a carbon fiber reinforced epoxy matrix laminated composite (AS4/3501-6) was used as adherends in the numerical simulations and the basic mechanical properties of the unidirectional material are tabulated in Table 2. More information on the mechanical behavior of AS4/3501-6 can be obtained in references [50,51].

2.2. Nonlinear Finite Element Modeling of SLJs

In the study, the ANSYS code version 10.0 was used and a 3-D nonlinear finite element code was established to assess the effects of the fiber orientation angle (θ) of the laminates on the stress distributions and the failure prediction in the SLJs subjected to uniaxial tensile loading. Eight different configurations were considered and the unidirectional prepregs were laid up in quasi-isotropic ($[90/\pm45/0]_{2s}$ and $[90/\pm30/90]_{2s}$), cross-ply ($[0/90]_{4s}$ and $[30/60]_{4s}$), angle-ply ($[45/-45]_{4s}$ and $[55/-55]_{4s}$), and unidirectional ($[0]_{16}$ and $[90]_{16}$). The ply thickness was 0.132 mm, thus the thickness of adherend was 2.11 mm. Consequently, the test specimens with finite element meshing are shown in Fig. 4, while the geometry, configuration, loading, and boundary conditions of the specimen analyzed are given in Table 3.

In the analysis, the 3-D 8-node layered structural solid element, SOLID 46, for the composite adherends, and the 3-D 8-node structural solid element, SOLID 185, for the adhesive, were used. SOLID 46

TABLE 2 Typical 3-D Mechanical Properties of AS4/3501-6 Carbon/Epoxy Composite Lamina [50,51]

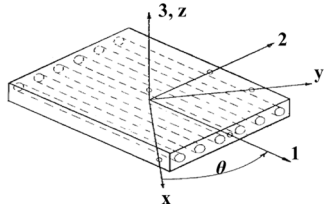

Property	Value
E_1; Tensile modulus in 1-direction	113.6 GPa
E_2, E_3; Tensile moduli in 2- and 3-directions, respectively	9.65 GPa
G_{12}, G_{13}; Shear moduli in 12- and 13-directions, respectively	6 GPa
G_{23}; Shear modulus in 23-direction	3.8 GPa
ν_{12}; Poisson's ratio in 12-directions	0.334
ν_{13}; Poisson's ratio in 13-directions	0.328
ν_{23}; Poisson's ratio in 23-directions	0.54
S^t_{11}; Tensile strength in 1-direction	1720 MPa
S^c_{11}; Compressive strength in 1-direction	1170 MPa
S^t_{22}, S^t_{33}; Tensile strengths in 2- and 3-directions, respectively	55.2 MPa
S^c_{22}, S^c_{33}; Compressive strengths in 2- and 3-directions, respectively	207 MPa
S_{12}; Shear strength in 12-directions	103 MPa
S_{13}, S_{23}; Shear strengths in 13- and 23-directions, respectively	82.7 MPa
Lamina thickness	0.13208 mm

allows up to 250 different material layers and the element has three degrees of freedom at each node: translations in the nodal x, y, and z directions. SOLID185 has three degrees of freedom at each

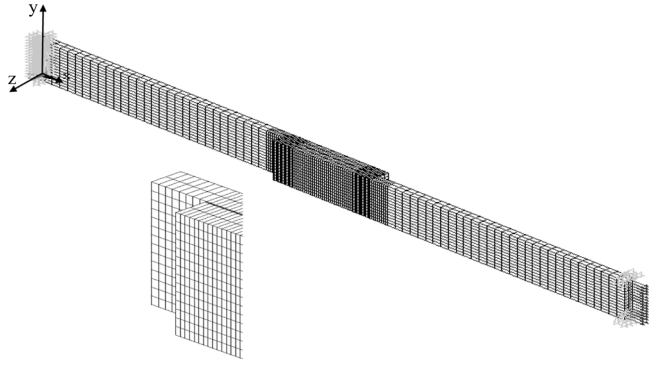

FIGURE 4 Mesh details, loading and boundary conditions for SLJ.

TABLE 3 Boundary Conditions and Geometrical Parameters Used in Numerical Studies (All Dimensions in mm)

Laminates	Lay-up
Angle ply	TA1: $[45/-45]_{4s}$
	TA2: $[55/-55]_{4s}$
Cross ply	TC1: $[0/90]_{4s}$
	TC2: $[30/60]_{4s}$
Unidirectional	TU1: $[0]_{16}$
	TU2: $[90]_{16}$
Quasi-isotropic	TQ1: $[90/\pm45/0]_{2s}$
	TQ2: $[90/\pm30/90]_{2s}$
Adherend thickness	2.11
Overlap length - l	25
Adhesive thickness - t	0.12
Adherend width	12.5

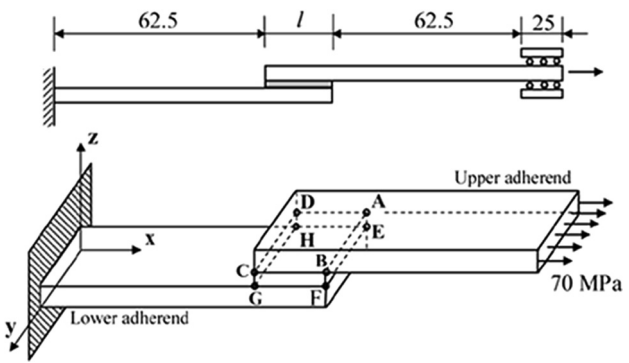

node: translations in the nodal x, y, and z directions and the element has plasticity, hyper-elasticity, stress stiffening, creep, large deflection, and large strain capabilities [35].

The adherends were modeled with two layers of SOLID 46 elements for SLJs subjected to the uniaxial tensile loading. Also, each of these solid elements was further modeled as an eight-layer material. The composite adherends (AS4/3501-6) were assumed to behave as linearly elastic materials while the adhesive layer (FM 73) was assumed to be nonlinear (see Section 2.1). The nonlinear geometric deformations of the SLJs were also taken into account. The material properties used for the purpose are given in Tables 1 and 2 as mentioned above.

In the case of the axial tensile loading of the joint, one end of the adherends was constrained from x, y, and z translation while the other end was constrained from y and z translation, as seen from the figure in Table 3 and Fig. 4. The load was applied in the form of pressure to this end towards the positive x-direction. The magnitude of pressure on a cross-section of 12.5×2.11 mm was 70 MPa.

3. RESULTS AND DISCUSSION

The present FE analysis results and earlier studies [26–31] have shown that the most critical regions are along the composite adherend–adhesive interfaces; there are several sites of anticipated high stress gradients and also several lines where a mathematical stress singularity is expected. Particularly, the following lines noted in the figure in Table 3 are under suspicion [28]:

- Lines AB, BC, CD, and DA which belong to the interface between upper adherend and adhesive,
- Lines EF, FG, GH, and HE which belong to the interface between lower adherend and adhesive.

The nature of expected singularity along the lines AB and GH on the interfaces along the free edges is different from the other six lines and the failure probably initiates from those corner lines, because the stress distributions are the highest here compared with any other locations. Also, the stress distributions on the lines AB and GH are almost identical. For this reason, corner line AB only is considered for the analyses (see figure in Table 3).

On the other hand, the normal and shear stress distributions along the corner line AB on the adhesive side obtained from FE analyses were normalized by dividing by the tensile ultimate strength and the shear strength of FM 73 ($\sigma_t = 55.4$ MPa, $\tau_y = 40.9$ MPa), respectively.

Also, all stress distributions along the line AB on the adherend side were normalized by dividing by the strength components (S_{ij}) of the composite material (Table 2).

The stress distributions of the adhesive side on the interface of the upper adherend–adhesive in the overlap region of SLJ with a stacking sequence of $[90]_{16}$, obtained from FE analyses, are presented in Fig. 5. Three-dimensional effects are indicated from this figure. There are three effects of 3-D deformation for laminated composite SLJs: (i) anti-clastic bending of adherends and Poisson effects; (ii) free edge effect; (iii) bending-twisting coupling effect. The anti-clastic effect is due to the different deformation between upper and lower surfaces of the composite laminates. Put another way, the upper and lower surfaces of the adherend deform in a convex (concave) manner in one direction and concave (convex) in the perpendicular direction when the joint is subjected to bending. The free edge effect is basically due to the mismatch of elastic properties of the joint materials. The state of stress in the vicinity of the free edge of the joint is fully 3-D which has not been taken into account in any classical theory so far.

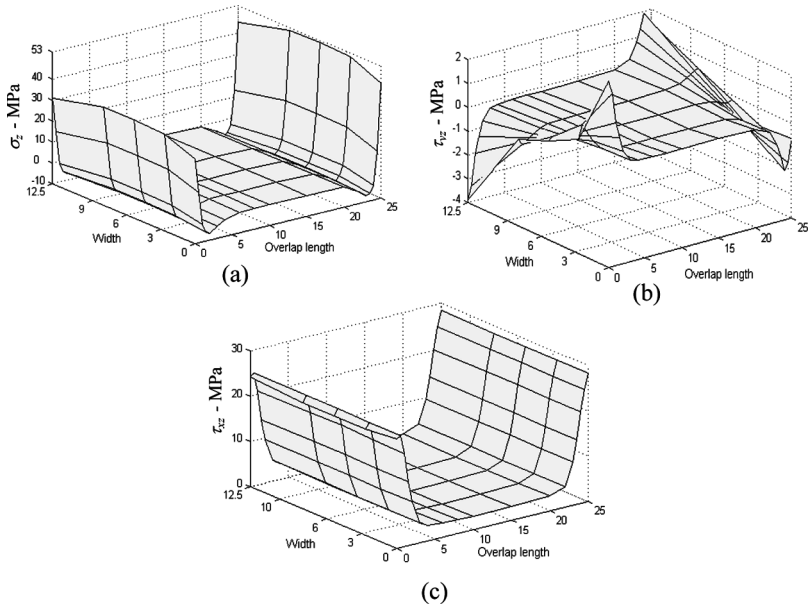

FIGURE 5 Peel and shear stress distributions of the adhesive side on the interface of upper adherend-adhesive for SLJ with a stacking sequence of $[90]_{16}$: (a) Peel stress σ_z, (b) Shear stress τ_{yz}, and (c) Shear stress τ_{xz}.

Also, the lamination constitutive relationships and coupling effect due to bending, twisting, and stretching give rise to a 3-D state of stress at the overlap region [26,31]. None of these effects can be captured when solving 2-D plane strain or plane stress problems and they cannot be neglected in the stress and failure analysis.

The peel stress distributions (σ_z) on the interface of the top adherend-adhesive in the overlap region of the joint and on the adhesive side are shown in Fig. 5a. It can be observed that σ_z is largest at the center of the joint and lowest at the edges. This is due to an anti-clastic effect and this effect reduces or suppresses the development of tensile peel stress at the corners, such as points A and B in the adhesive layers [26].

Polymer matrix composite adherends are considerably more affected by interlaminar shear stresses than metals, so that there is a significant need to account for such effects in stress analyses of adhesively bonded composites. Figures 5b and 5c show the out-of-plane shear stress distributions. Again, the 3-D effects are observed and it is clearly seen from Fig. 5b that the shear stress distribution in the yz direction (τ_{yz}) is more sensitive to the 3-D effects compared with other stress distributions (σ_z and τ_{xz}). Also, there is a strong stress concentration effect at the two corners of the free edge of the overlap (Fig. 5b).

3.1. Effect of Ply Stacking Sequence

3.1.1. Stress Distributions on the Adhesive Layer

The normal and shear stress distributions along the line AB on the adhesive side for the SLJs consisting of composite adherends with various ply stacking sequences are shown in Figs. 6 and 7. It can clearly be seen that the fiber orientation has a significant effect on all the stress distributions (Figs. 6 and 7).

Figure 6 shows the shear stress distributions in the yz and xz directions (τ_{yz}, τ_{xz}) along the line AB. The 3-D effects are shown in this figure and it is clearly seen in Fig. 6a that the shear stress distribution in the yz direction (τ_{yz}) along the line AB on the adhesive side is more sensitive to the 3-D effect for the SLJs with laminates $[45/-45]_{4s}$, $[55/-55]_{4s}$ and $[30/60]_{4s}$. In addition, there is a strong stress concentration effect at the two corners of the free edge of the overlap, especially for the SLJs with laminates $[45/-45]_{4s}$ and $[55/-55]_{4s}$ (Fig. 6a).

Figure 7 shows the maximum normal stress components (σ_x, σ_y, and σ_z) along the line AB (see figure, Table 3). The peel stress (σ_z) at the free ends of the overlap is very important as it causes initiation of a crack in this region (Fig. 7c). The other normal stress components are largest at the center of the joint and lowest at the edges except

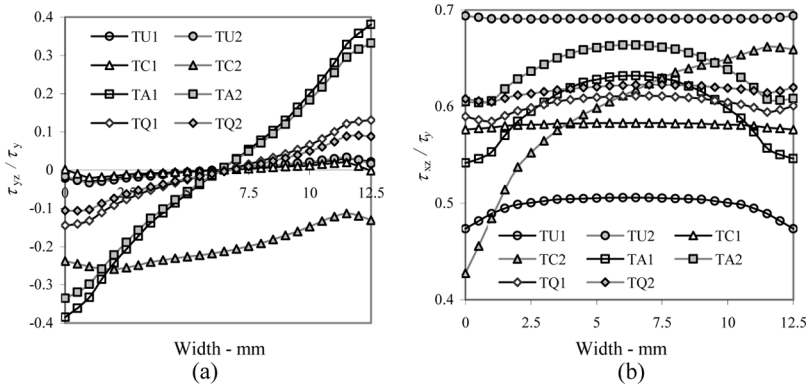

FIGURE 6 Shear stress distributions, normalized to the shear strength of FM 73 (τ_y), along the line AB (see Table 3) on the adhesive side (TU1:$[0]_{16}$, TU2:$[90]_{16}$, TC1:$[0/90]_{4s}$, TC2:$[30/60]_{4s}$, TA1:$[45/-45]_{4s}$, TA2:$[55/-55]_{4s}$, TQ1:$[90/\pm45/0]_{2s}$ and TQ2:$[90/\pm30/90]_{2s}$): (a) Normalized shear stress τ_{yz} and (b) Normalized shear stress τ_{xz}.

for SLJs with laminate $[30/60]_{4s}$. It is noticed that the stress distributions are constant for most of the overlap portion except at the edges. This is due to the 3-D effects (anti-clastic, free edge, and bending–twisting effects) which reduce or suppress the development of the normal stress at the corners in the adhesive layer, especially for SLJs with laminates $[45/-45]_{4s}$, $[55/-55]_{4s}$, and $[30/60]_{4s}$. At the same time, the maximum normal stress distributions occur in the SLJs with laminates $[90]_{16}$, $[45/-45]_{4s}$, $[55/-55]_{4s}$, and $[30/60]_{4s}$ while the minimum normal stress distributions occur in the SLJs with laminates $[0]_{16}$ and $[0/90]_{4s}$ owing to the fact that the layers, except for the 0° degree layer on outer surfaces, tend to seriously weaken the stiffness of the joint, especially the bending stiffness (Fig. 7).

Consequently, it can be stated that the SLJs with laminates $[0]_{16}$ and $[0/90]_{4s}$ have lower normal and shear stress distributions, especially peel stress, than the others (Figs. 6 and 7) because 0° layers next to the bond layer give stiffer adherend response.

3.1.2. Stress Distributions on the Composite Adherends

The normal and shear stress distributions along the line AB on the adherend side are shown in Fig. 8, for the SLJs consisting of composite adherends with various fiber orientation angles. The fiber orientation has a significant effect on the maximum stress. The magnitudes of the maximum axial and peel stresses are smaller than the strengths in the x and z directions, respectively (Table 2). On the other hand, the maximum

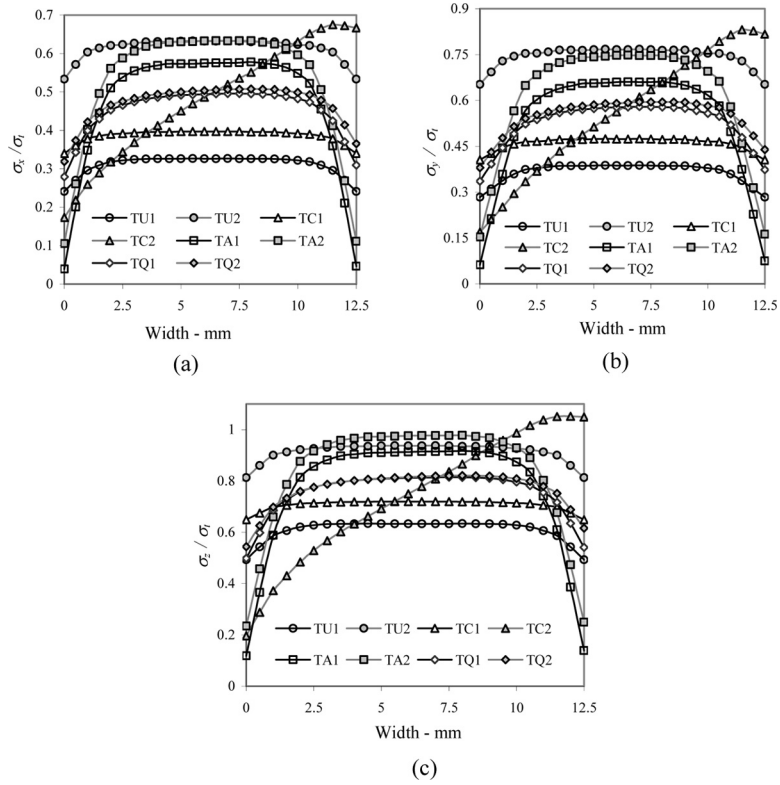

FIGURE 7 Normal stress distributions, normalized to the tensile ultimate strength of FM 73 (σ_t), along the line AB (see Table 3) on the adhesive side (TU1:$[0]_{16}$, TU2:$[90]_{16}$, TC1:$[0/90]_{4s}$, TC2:$[30/60]_{4s}$, TA1:$[45/-45]_{4s}$, TA2:$[55/-55]_{4s}$, TQ1:$[90/\pm45/0]_{2s}$ and TQ2:$[90/\pm30/90]_{2s}$): (a) Normalized stress σ_x, (b) Normalized stress σ_y, and (c) Normalized stress σ_z.

normal transverse stress (σ_y) and shear stress in the xy direction (τ_{xy}) occur in the SLJs with laminates $[45/-45]_{4s}$, $[55/-55]_{4s}$, and $[30/60]_{4s}$ and the magnitudes of those stresses (σ_y and τ_{xy}) are much higher than the strengths in the y direction and shear strength in the xy directions, respectively (Figs. 8b and 8d). Hence, from the finite element analyses, it can be stated that the failure on laminates $[45/-45]_{4s}$, $[55/-55]_{4s}$, and $[30/60]_{4s}$ are due to the maximum stress σ_y and shear stress τ_{xy}. As seen from Fig. 8, 3-D effects on the normal and shear stress components in SLJs with composite adherends are observed, again.

As a result, neglecting the out-of-plane stress distributions would result in an inaccuracy in the analysis of composite laminated joints.

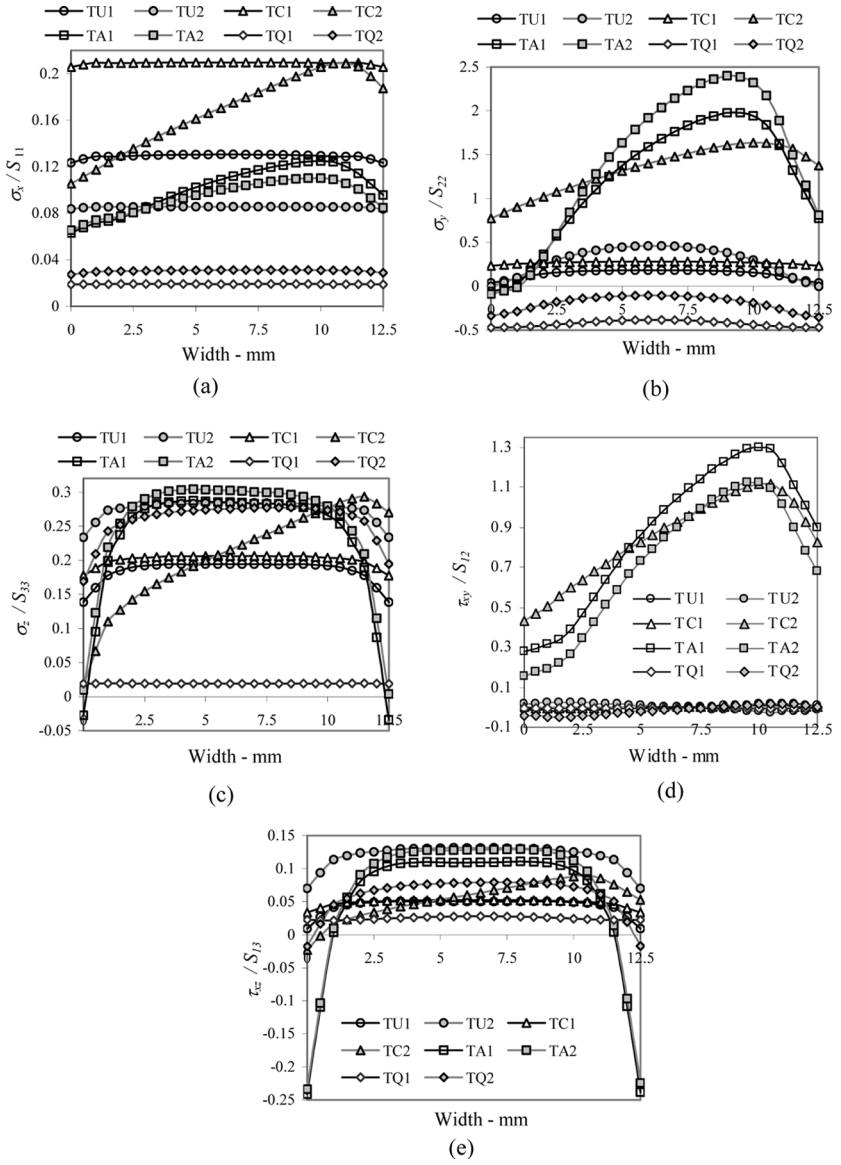

FIGURE 8 Stress distributions, normalized by dividing with the strength components (S_{ij}) of the composite material, along the line AB (see Table 3) on the adherend side (TU1:$[0]_{16}$, TU2:$[90]_{16}$, TC1:$[0/90]_{4s}$, TC2:$[30/60]_{4s}$, TA1:$[45/-45]_{4s}$, TA2:$[55/-55]_{4s}$, TQ1:$[90/\pm45/0]_{2s}$ and TQ2:$[90/\pm30/90]_{2s}$): (a) Normalized stress σ_x, (b) Normalized stress σ_y, (c) Normalized stress σ_z, (d) Normalized shear stress τ_{xy}, and (e) Normalized shear stress τ_{xz}.

Hence, the out-of-plane stresses (the shear stress in the xy direction, etc.) and 3-D effects cannot be neglected in the stress and failure analysis.

3.1.3. Strength Characteristics of Adhesive and Adherends

Using Eqs. (1) and (3), failure indexes (e, e_{com}) are calculated for the composite adherend and adhesive layer, respectively. Failure indexes are defined as the parameters predicting the strength of the joint. In order to avoid failure, e, e_{com} for both the adhesive and the composite adherends must be less than 1; failure is predicted when e or e_{com} are ≥ 1. The distributions of e on the adherend-adhesive interface in the overlap region of the joint and on the adhesive side are shown in Figure 9. As seen from this figure, the minimum e distributions occur in the SLJs with laminates $[0]_{16}$ and $[0/90]_{4s}$ and the possibility of failure initiation would be from the interface of the top adherend-adhesive along the free edge, in order that the value of e is the highest here compared with any other locations.

On the other hand, the most critical points for composite adherends are the interface of the top adherend-adhesive along the free edge, also. Hence, the line AB was considered in order to compare with failure indexes of composite adherends. As seen from Figs. 10a and 10b, failures along the line AB on the laminates $[0]_{16}$, $[90]_{16}$, $[0/90]_{4s}$, $[90/\pm 45/0]_{2s}$, and $[90/\pm 30/90]_{2s}$ do not occur while the failure along the line AB on the laminates $[45/-45]_{4s}$, $[55/-55]_{4s}$, and $[30/60]_{4s}$ occur, under the same load.

Consequently, for both the adherends and the adhesive layer, it can clearly be stated that the SLJs with laminates $[0]_{16}$ and $[0/90]_{4s}$ have lower normal and shear stress distributions, especially peel stress, than the others because 0° layers next to the bond layer give stiffer adherend response.

4. CONCLUSIONS

This study has dealt with the effects of the fiber orientation angles of the laminates on the stress distributions and the failure prediction in the SLJs subjected to uniaxial tensile loading *via* a 3-D non linear finite element method. The results obtained are as follows:

- It was seen that the state of stress in the vicinity of the free edge of the joint is fully 3-D which has not been taken into account in any classical theory so far and that the normal and shear stress distributions are extremely sensitive to these 3-D effects (anti-clastic, free edge, and bending-twisting coupling effects).

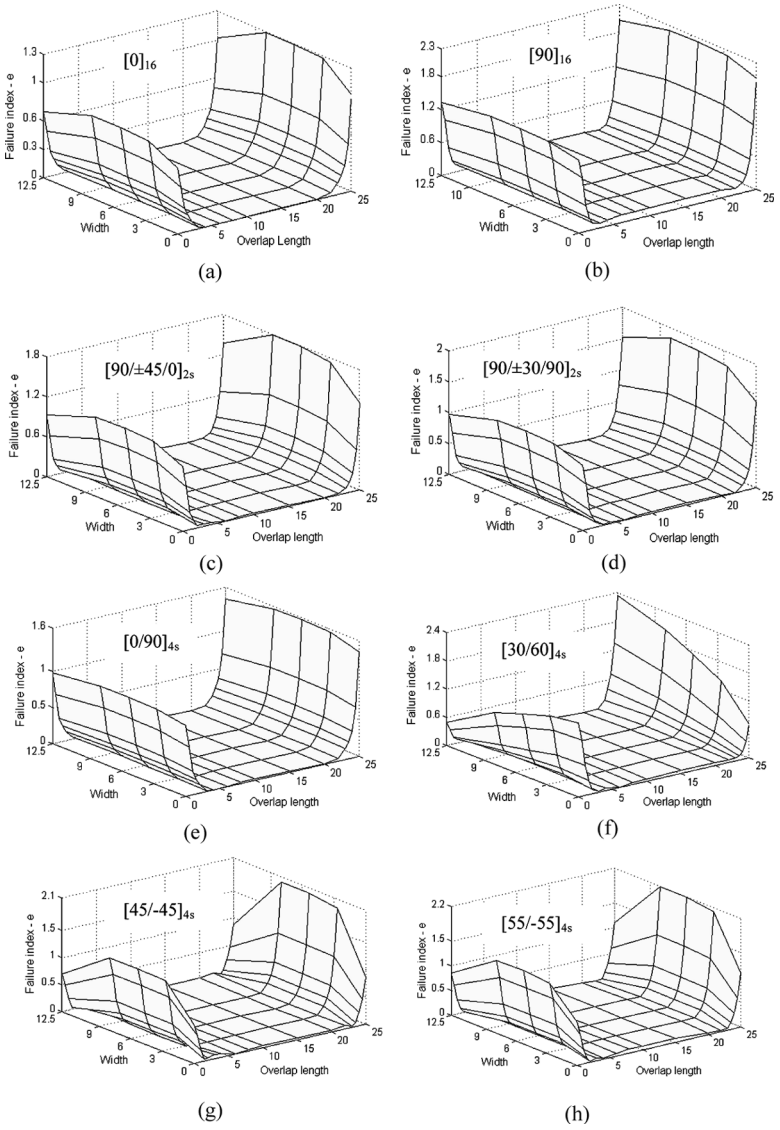

FIGURE 9 Failure index distributions (e) on the interface of top adherend-adhesive in the SLJs consisting of composite adherends with various fiber orientation angles and on the adhesive side: (a) for SLJ with laminate $[0]_{16}$, (b) for SLJ with laminate $[90]_{16}$, (c) for SLJ with laminate $[90/\pm45/0]_{2s}$, (d) for SLJ with laminate $[90/\pm30/90]_{2s}$, (e) for SLJ with laminate $[0/90]_{4s}$, (f) for SLJ with laminate $[30/60]_{4s}$, (g) for SLJ with laminate $[45/-45]_{4s}$, and (h) for SLJ with laminate $[55/-55]_{4s}$.

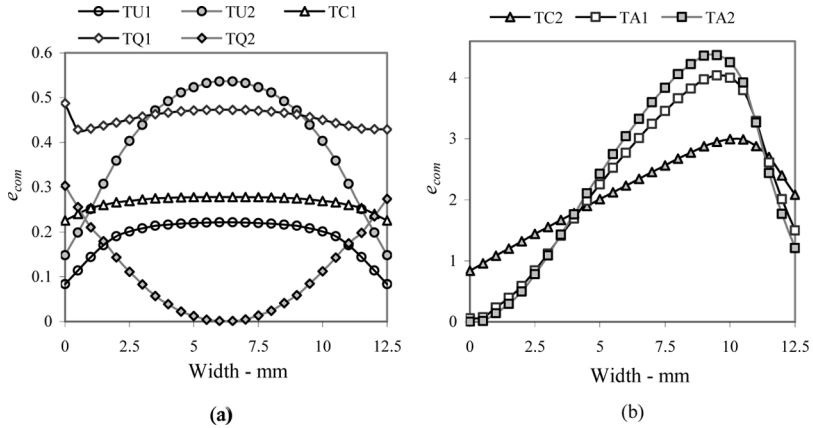

FIGURE 10 Failure index distributions (e_{com}) along the line AB on the adherend side (TU1:$[0]_{16}$, TU2:$[90]_{16}$, TC1:$[0/90]_{4s}$, TC2:$[30/60]_{4s}$, TA1:$[45/-45]_{4s}$, TA2:$[55/-55]_{4s}$, TQ1:$[90/\pm45/0]_{2s}$ and TQ2:$[90/\pm30/90]_{2s}$).

- Neglecting the out-of-plane stress distributions would result in inaccurate static strength predictions in the analysis of composite laminated joints. Hence, in real applications of adhesively bonded composite joints, the out-of-plane stresses and 3-D effects cannot be neglected in the stress and failure analysis and a 3-D finite element method is essential to evaluate explicitly the stress and failure states.
- The peel stress (σ_z) is largest at the center of the joint and lowest at the edges. This is due to the anti-clastic effect and this effect reduces or suppresses the development of tensile peel stress at the corners in the adhesive layers.
- The fiber orientation and ply stacking sequence have a significant effect on the stress distribution and the failure. For both the adherends and the adhesive layer, the stress distributions in the SLJs with laminates $[0]_{16}$ and $[0/90]_{4s}$ are lower than the others because 0° layers next to the bond layer give stiffer adherend response, especially higher bending stiffness.

REFERENCES

[1] Içten, B. M. and Karakuzu, R., *Composites Sci. Technol.* **62**, 1259–1271 (2002).
[2] Mortensen, F. and Thomsen, O. T., *Composite Structures* **56**, 165–174 (2002).
[3] Volkersen, O., *Luftfahrtforschung* **15**, 41–47 (1938).
[4] Goland, M. and Reissner, E., *J. Appl. Mech.* **11**, 17–27 (1944).

[5] Hart-Smith, L. J., Adhesive bonded single lap joints, NASA Report CR-112236 (Langley Research Center, Hampton, VA, 1973).
[6] Oplinger, D. W., *Int. J. Solids Struct.* **31**, 2565–2587 (1994).
[7] Adams, R. D. and Peppiatt, N. A., *J. Strain Anal.* **8**, 134–139 (1973).
[8] Adams, R. D. and Peppiatt, N. A., *J. Strain Anal.* **9**, 185–196 (1974).
[9] Chen, D. and Cheng, S., *J. Eng. Mech.* **35**, 55–73 (1983).
[10] Tsai, M. Y., Oplinger, D. W., and Morton, J., *Int. J. Solids Struct.* **35**, 1163–1185 (1998).
[11] Crocombe, A. D. and Bigwood, D. A., *J. Strain Anal.* **27**, 211–218 (1992).
[12] Odi, R. A. and Friend, C. M., *Int. J. Adhesion Adhesives* **24**, 389–405 (2004).
[13] Wooley, G. R. and Carver, D. R., *J. Aircraft* **8**, 17–20 (1971).
[14] Chen, D. and Cheng, S., *J. Appl. Mech.* **50**, 109–115 (1983).
[15] Harris, J. A. and Adams, R. D., *Int. J. Adhes. Adhes.* **4**, 65–78 (1984).
[16] Carpenter, W. C. and Barsoum, R., *J. Adhesion* **30**, 25–46 (1989).
[17] Richardson, G., Crocombe, A. D., and Smith, P. A., *Int. J. Adhes. Adhes.* **13**, 193–200 (1993).
[18] Sheppard, A., Kelly, D., and Tong, L., *Int. J. Adhes. Adhes.* **18**, 385–400 (1998).
[19] Andruet, R. H., Dillard, D. A., and Holzer, S. M., *Int. J. Adhes. Adhes.* **21**, 17–34 (2001).
[20] Gonçalves, J. P. M., de Moura, M. F. S. F., and de Castro, P. M. S. T., *Int. J. Adhes. Adhes.* **22**, 357–365 (2002).
[21] Apalak, M. K. and Engin, A., *J. Adhesion Sci. Technol.* **17**, 1889–1922 (2003).
[22] Ozel, A., Aydin, M. D., and Temiz, Ş., *J. Adhesion Sci. Technol.* **18**, 313–325 (2004).
[23] Aydin, M. D., Ozel, A., and Temiz, Ş., *J. Adhesion Sci. Technol.* **19**, 705–718 (2005).
[24] Magalhaes, A. G., de Moura, M. F. S. F., and Gonçalves, J. P. M., *Int. J. Adhes. Adhes.* **25**, 313–319 (2005).
[25] Wang, C. H. and Rose, L. R. F., *Int. J. Adhes. Adhes.* **17**, 17–25 (1997).
[26] Tsai, M. Y., Morton, J., and Matthews, F. L., *J. Composite Mat.* **29**, 1254–1275 (1995).
[27] Adams, R. D. and Davies, R., *J. Adhesion* **59**, 171–182 (1996).
[28] Bogdanovich, A. E. and Kizhakkethara, I., *Composites Part B* **30**, 537–551 (1999).
[29] Kaye, R. and Heler, M., *Int. J. Adhes. Adhes.* **26**, 261–273 (2006).
[30] Chan, W. S. and Vedhagiri, S., *J. Composite Mat.* **35**, 1045–1061 (2001).
[31] Panigrahi, S. K. and Pradhan, B., *J. Reinforced Plastics and Comp.* **26**, 183–201 (2007).
[32] Tsai, S. W. and Hahn, H. T., *Introduction to Composite Materials* (Technomic Publishing Company, Lancaster, PA, USA, 1980), Section 7.2.
[33] Drucker, D. C. and Prager, W., *Quarterly of Applied Mathematics* **10**, 157–165 (1952).
[34] Raghava, R. S., Cadell, R. M., and Yeh, G. S., *J. Mater. Sci.* **8**, 225–232 (1973).
[35] ANSYS®, The General Purpose Finite Element Software (Version 10.0), Swanson Analysis Systems Inc., Houston, Texas.
[36] Dean, G. D. and Crocker, L. E., *Comparison of the Measured and Predicted Deformation of an Adhesively Bonded Lap-joint Specimen, NPL CMMT(A) 293* (National Physical Laboratory, Teddington, UK, 2000).
[37] Read, B. E., Dean, G. D., and Ferriss, D. H., *An Elastic-Plastic Model for the Non-Linear Mechanical Behaviour of Rubber-Toughened Adhesives, NPL CMMT(A) 289* (National Physical Laboratory, Teddington, UK, 2000).
[38] Broughton, W. R., Crocker, L. E., and Urquhart, J. M., *Strength of Adhesive Joints: A Parametric Study, NPL MATC(A) 27* (National Physical Laboratory, Teddington, UK, 2000).

[39] Dean, G. D., Crocker, L., Read, B., and Wright, L., *Int. J. Adhes. Adhes.* **24**, 295–306 (2004).
[40] Zgoul, M. and Crocombe, A. D., *Int. J. Adhes. Adhes.* **24**, 355–366 (2004).
[41] Charalambides, M. N. and Olusanya, A., *The Constitutive Models Suitable for Adhesives in some Finite Element Codes and Suggested Methods of Generating the Appropriate Materials Data, NPL CMMT(B)130* (National Physical Laboratory, Teddington, UK, 1997).
[42] Adams, R. D., *J. Adhesion* **30**, 219–242 (1989).
[43] Duncan, B. C., Girardi, M. A., and Read, B. E., *The Preparation of Bulk Adhesive Samples for Mechanical Testing, NPL Report DMM (B) 339* (National Physical Laboratory, Teddington, Middlesex, UK, 1994).
[44] ISO 15166-2: Adhesives-Methods of preparing bulk specimens, Part 2: Elevated-temperature-curing one-part systems (2000).
[45] ISO 527-2: Plastics-Determination of tensile properties, Part 2: Test conditions for moulding and extrusion of plastics (1993).
[46] ISO 527-1: Plastics-Determination of Tensile Properties, Part 1: General Principles (1993).
[47] Chiu, W. K., Chalkley, P. D., and Jones, R., *Computers and Structures* **53**, 483–489 (1994).
[48] Chiu, W. K. and Jones, R., *Int. J. Adhes. Adhes.* **15**, 131–136 (1995).
[49] Chun, H. W. and Chalkley, P. D., *Int. J. Adhes. Adhes.* **20**, 155–164 (2000).
[50] Daniel, I. M. and Abot, J. L., *Composites Sci. Technol.* **60**, 2455–2463 (2000).
[51] Camponeschi, E. T., *Compression Response of Thick-Section Composite Materials*, DTRC-SME-90/60, (David Taylor Research Center, Annapolis, USA, 1990).